RESEARCH PAPER

Effect of Zr Content on Oxide-scale Spallation of Aluminide Coating

R. Latifi, S. Rastegari* and S.H. Razavi

* *rastegari@iust.ac.ir*

Received: December 2018 **Revised: June 2019** **Accepted: August 2019**

School of Metallurgy and Materials Engineering, Iran University of Science and Technology, Tehran 16844, Iran.

DOI: 10.22068/ijmse.16.4.63

Abstract: *In the present study, zirconium modified aluminide coating on the nickel-base superalloy IN-738LC was first created by high activity high temperature aluminizing based on the out-of-pack cementation method. Then, Zr coatings were applied to simple aluminide coatings by sputtering and heat treatment in order to study the effect of Zr on the coating microstructure and oxide spallation. Microstructural studies were conducted by using scanning electron microscopy (SEM), energy dispersive X-ray spectrometry (EDS), and X-ray diffraction (XRD) microanalysis. The results indicated that zirconium modified aluminide coating, like aluminide coating, has a two-layer structure including a uniform outer layer of NiAl and an interdiffusion layer in which zirconium is in a form of solid solution in the coating. Furthermore, the 300 nm Zr-coated NiAl demonstrated an excellent scale adhesion, a slow oxidation rate and lower amounts of other elements such as Ti and Cr in its oxide layer lead to a pure aluminide oxide layer.*

Keywords: *Diffusion aluminide coating, Zirconium modified coating, Oxidation resistance, Out-of-pack cementation.*

1. INTRODUCTION

In many technological applications, coatings are used to protect the parts against environmental failures. During the past decades, diffusion aluminide coatings have been widely implemented in the hot section of the jet engines and turbine blades as both protective coatings and bond coats in the thermal barrier coating (TBC) system. In the TBC system, the bond coat has attracted a lot of attention due to its ability to form a protective aluminide oxide layer in the oxidizing environment of industrial and aero-gas turbines [1]. One of the key factors in reducing the delamination of the ceramic topcoat and TBC failure is related to the adhesion of this oxide layer or TGO (thermally grown oxide), which determines the ultimate lifetime of TBC. However, alumina scale adhesion is sensitive to impurities such as S and spalls easily during high-temperature operations, especially above 1200 °C [2]. The adhesion of the α-Al_2O_3 layer to the coating is influenced by some parameters such as the chemical composition of the coating. Previous studies have demonstrated that the addition of small amounts of reactive elements such as Pt, Hf, Dy, and Zr to β-NiAl plays a significant role in the high-temperature oxidation of the alloys as well as improving the lifetime of the system [3-7]. The adhesion strength of the bond coat and oxide layer should be increased in order to avoid spalling the oxide layer [8-9]. Zr is considered as one of the most effective elements in improving the adhesion of alumina layer since it can reduce the formation of holes in the interface of the substrate and the coating. In addition, it can prevent from segregating sulfur in the mentioned holes [10]. Further, some studies indicated that Zr inhibits the outward diffusion of Al during oxidation and accordingly decelerates the growth rate of oxide scale [5, 11, 12]. Doping aluminide coatings with Zr can significantly influence on cyclic oxidation behavior and it is regarded as an affordable coating for industrial applications, compared to Pt-modified aluminide coatings. To date, several efforts have been conducted for modifying aluminide coating via Zr by pack cementation [3], vapor phase deposition [5], and the CVD method [4].

In the present study, the out-of-pack cementation method was used for creating aluminide diffusion coating and Zr was deposited by a sputtering method with two thicknesses. In contrast to in-pack cementation, out-of-pack does not result in including pack materials such as alumina in the produced coatings [13]. This

[DOI: 10.22068/ijmse.16.4.63]

method can lead to a cleaner and uniform coating for very complicated geometry components, without any entrapped pack particles [14]. The present study aimed to emphasize the role of zirconium and its content in cyclic oxidation behavior of NiAl coating via enhancing the adhesion between the alumina scale and coating and decreasing the scale detachment which has not been reported elsewhere.

2. MATERIALS

As shown in Table 1, IN-738LC was first prepared as a base material with chemical composition. Then, the samples with the dimensions of 10*10 mm and thickness of 3 mm were grounded up to SiC No 1000 and ultrasonically cleaned in acetone. In the next procedure, aluminizing by the out-of-pack cementation method was conducted under an argon atmosphere by using a powder mixture including Al (15 wt-%) and NH_4Cl (2 wt-%) as an activator and Al_2O_3 (83 wt-%) at 1050°C for 4 h. In addition, the sputtering machine (Sputter-MMs-160, 460v, 210 A and $4.5*10^{-3}$ mbar pressure) was used to deposit Zr at 100 and 300 nm thickness. Further, the coated specimens were annealed at 1050 °C for 3 h under flowing Ar in order to diffuse Zr and obtain a homogeneous coating composition. The oxidation resistance of samples was studied at 1000 °C for 120 h in the air atmosphere. Each cycle consists of heating up to 1000 °C for 24 h and then 1 h cooling down to ambient temperature. Furthermore, the mass change was measured by using microbalance, which was determined based on an average value of three specimens for each coating condition. Finally, TESCAN scanning electron microscopy (SEM), elemental analysis (EDS), and X-ray diffraction (XRD) were used to evaluate the effects of processing parameters on the microstructural properties and oxidation behavior of the coatings. In addition, encoding samples were used to facilitate the description of the coating conditions (Table 2).

3. RESULTS AND DISCUSSION

3.1. Microstructure of NiAl and Zr-Coated NiAl

Fig. 1 illustrates the cross-section of all coatings after fabrication including NiAl coating (AHHZ0), the 100 nm Zr-coated NiAl (AHHZ10), and the 300 nm Zr-coated NiAl (AHHZ30). Due to similar conditions for the aluminizing process for all samples, the produced coating is uniform and is generally composed of an external layer and the interdiffusion region in which the minimum and maximum thickness are achieved in AHHZ0 (10 and 14 μm) and AHHZ30 (14 and 18 μm), respectively. However, the thickness of the coating does not change significantly because the time and temperature are the same for the process of aluminizing. As shown in Table 3, the outer layer is composed of Ni-rich NiAl phase based on the chemical composition of these coatings. Regarding the concentration of Ni and Al in different regions in the coating, it is observed that

Table 1. Chemical composition of IN738-LC (wt-%).

Cr	Co	Al	Ti	Ta	W	Mo	Nb	Zr	C	B	Ni
16	8.5	3.4	3.4	1.7	2.6	1.7	0.9	0.05	0.11	0.01	Bal.

Table 2. Encoding of various coated samples.

Method of coating deposition	sample	Zr thickness (nm)
Out-of-pack cementation aluminizing	AHHZ0	0
Out-of-pack cementation aluminizing, Zr 100 nm deposited by sputtering, heat treatment	AHHZ10	100
Out-of-pack cementation aluminizing, Zr 300 nm deposited by sputtering, heat treatment	AHHZ30	300

[DOI: 10.22068/ijmse.16.4.63]

the nickel outward diffusion from the substrate was more than the aluminum inward diffusion from the surface to the substrate. Consequently, Ni-rich NiAl grows outwardly and the Al-rich regions decrease gradually. Therefore, high activity process and heat treatment resulted in forming a Ni-rich NiAl phase [15]. The XRD analysis in Fig. 2 revealed that outer layer consists of NiAl and Ni_3Al phases. In addition, the absence of the matrix carbides in the outer layer of the coating revealed the outside growth in this region for each of the three samples [16, 17].

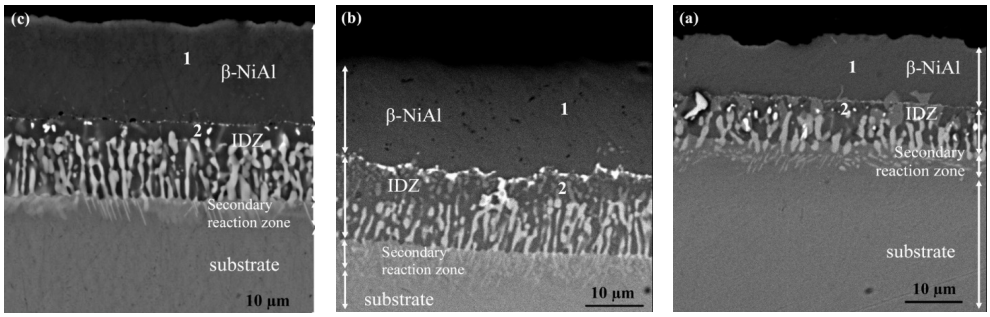

Fig. 1. Backscattered electron images of the cross section of NiAl coating after deposition and heat treatment for 3h at 1050°C (a) without Zr (AHHZ0) (b) 100 nm Zr-coated (AHHZ10) (c) 300nm Zr-coated (AHHZ30).

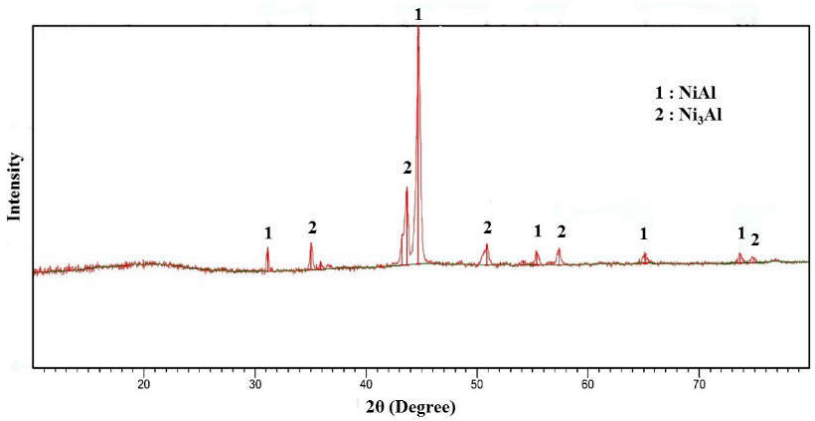

Fig. 2. The XRD patterns of the simple aluminide coating, AHHZ0.

Table 3. Chemical analysis of the cross-section of coated samples AHHZ0, AHHZ10 and AHHZ30 corresponding to the fig. 1 (at-%).

sample	region	Al	Ni	Ti	Cr	Co	Mo	W	Zr
AHHZ0	1	45.9	43.8	1.1	5.5	3.7	0	0	0
	2	40.7	41.4	4.5	5.9	4.3	2.1	0.8	0
AHHZ10	1	47.5	47.3	0	1.5	2.2	0	0	1.45
	2	37.2	32	6	15	2.6	0	1.8	4.8
AHHZ30	1	48.9	45.8	0	1.1	1.6	0	0	2.5
	2	43.2	39.1	3.2	3.4	2.2	0	0	8.9

[DOI: 10.22068/ijmse.16.4.63]

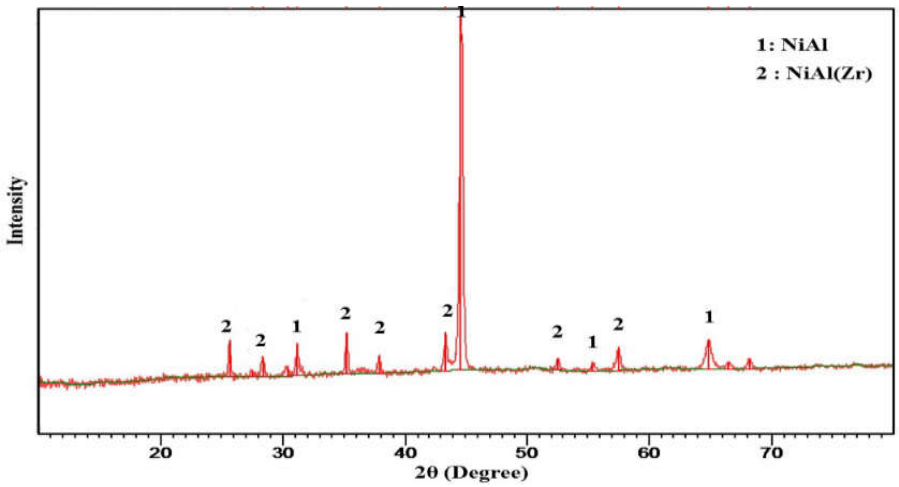

Fig. 3. The XRD patterns of the 100 nm Zr coated (AHHZ10).

Further, there are columnar structures with some light-colored precipitations in the interdiffusion region. Based on the results of some studies, the concentration of Ni in this region increased due to the diffusion of Ni from the middle of the substrate to the coating [18, 19]. Furthermore, accordingly the solubility of the heavy elements such as Cr, Mo, and W decreased in this region, which can be related to the formation of precipitations of heavy elements in this region. EDS microanalysis for the samples AHHZ10 and AHHZ30 demonstrated this phenomenon in the interdiffusion region (Tables 3). Based on the chemical analysis of region 1, it is observed that there is some Zr in the vicinity of Ni and Al. In region 2, the maximum value of Zr (0.8 and 1.6 at.%) is observed near the interface of the coating and the diffusion region. The XRD results shown in Fig. 3 indicate that the 100 nm Zr coated in the surface is distributed in the NiAl as a solid solution. The NiAl phase (with the crystal structure of CsCl type C) consisted of about 45-60 at.% of Ni with large non-stoichiometric regions. Equal numbers of Al and Ni atoms are in the corner and the center of the cube, respectively [20]. However, there is the probability of the replacement of Ni atoms with Zr in Ni-rich phase, and Zr may form substitutional solid solution in NiAl.

Fig 4. illustrates the line scan chemical analysis of the AHHZ30 coating sample. As observed, Zr is distributed in the aluminide coating region due to heat treatment which is in agreement with Hamadi et al [21] investigation.

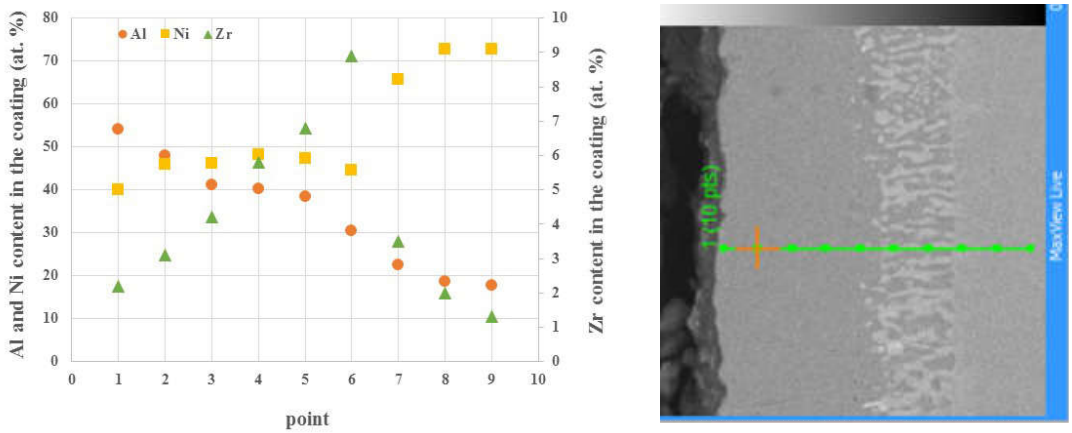

Fig. 4. Line scan of the cross section of AHHZ30 sample.

[DOI: 10.22068/ijmse.16.4.63]

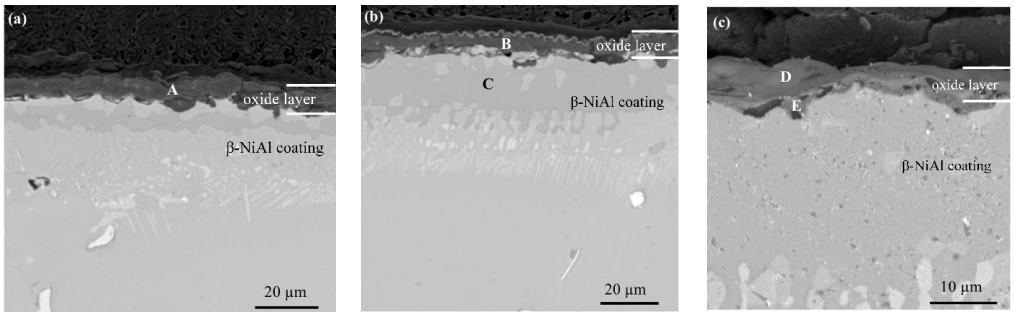

Fig. 5. SEM micrographs (Backscattered mode) of cross section of the samples a) AHHZ0 b) AHHZ10 and c) AHHZ30 after the hot oxidation at 1000°C for 120 h.

3.2. The Effects of Zr on the high temperature Oxidation Behavior of Aluminide Coating

Fig. 5 displays the SEM micrograph of AHHZ0, AHHZ10 and AHHZ30 samples, oxidized at 1000 °C for 120 h. Table 4 indicates the corresponding EDS microanalysis. Based on the EDS results, an Al_2O_3 oxide layer is formed in A, B, and D regions for the AHHZ0, AHHZ10 and AHHZ30 samples, respectively.

As illustrated in Fig. 6a, which is the SEM micrograph of the AHHZ0 sample after 120 h cyclic oxidation at 1000 °C, the surface of the coating is detached leading to the formation of different regions. Region 1 represents the protective aluminum oxide. In region 2, the aluminum content reduced to 22.6 % and it can be predicted that oxide is composed of these elements by regarding the presence of Ni, Cr, and Ti. In addition, the probability of the spallation in this region is higher due to the higher stability of aluminum oxide, compared to Cr, Ti and Ni oxides. Based on the microanalysis of region 3, the oxide layer is completely detached from the surface and a reduction occurs in the aluminum content in the coating during the oxidation cycle because of oxide formation. Thus, it can be expected that a layer of Ni_3Al is established here (Table 5).

Table 4. Chemical analysis of the cross-section of coated samples AHHZ0, AHHZ10 and AHHZ30 corresponding to the fig. 5 after 120 h oxidation at 1000°C (at-%).

sample	area						
		Al	Ni	Ti	Cr	Co	O
AHHZ0	A	34.1	1.1	2.7	1.3	0.2	60
AHHZ10	B	35	0.4	0.7	0.4	0	63
	C	31	53	5	3	5	0
AHHZ30	D	45.1	0.75	0.39	0.24	0.3	52.4
	E	35.7	0.5	0.4	0.1	0.1	59

Table 5. Chemical analysis of the cross-section of coated samples AHHZ0 and AHHZ10 corresponding to Fig. 6 after 120 h oxidation at 1000°C (at-%).

sample	area							
		Al	Ni	Ti	Cr	Co	O	Zr
AHHZ0	1	33	0.4	0.7	0.5	0	65	0
	2	22.6	4.8	2.2	4.2	1.3	64	0
	3	23	62	1.7	3.4	0	0	0
AHHZ10	1	29	0.9	0.7	0.3	0	60	7.8
	2	28	3.3	1.7	2	0.9	63	0
	3	36	51	2.5	5.4	4.6	0	0

[DOI: 10.22068/ijmse.16.4.63]

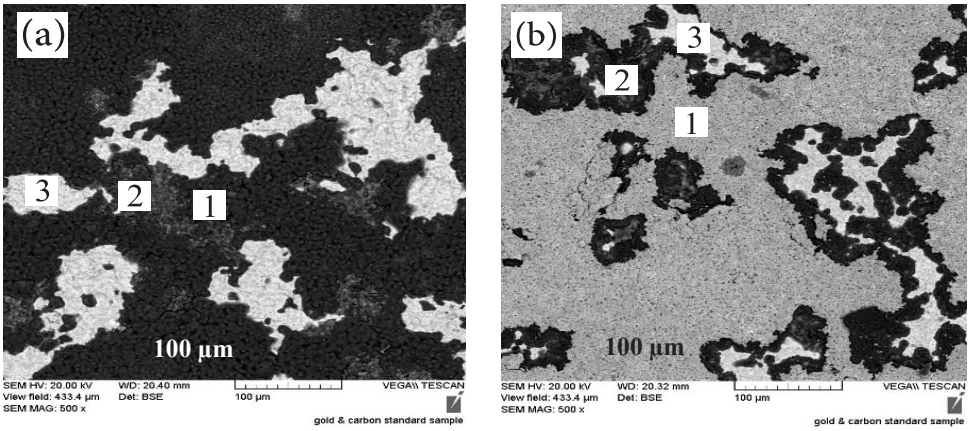

Fig. 6. SEM micrograph of the coated surface corresponding to the samples a) AHHZ0 and b) AHHZ10 after 120 hours of the hot oxidation at 1000°C.

SEM micrograph of the AHHZ10 sample after 120 h cyclic oxidation at 1000 °C reveals a little spallation and scaling on the surface (Fig. 6b). Based on the EDS microanalysis of the surface (Table 5), aluminum, zirconium, and oxygen are presented in region 1, which means that a continuous oxide layer with Zr and Al elements is formed. There are Al and O and a few Ni constituents in region 2, which experienced scaling during the cooling in the oxidation cycle. However, the oxide layer was formed again, which is expected to involve Al_2O_3 and NiO according to the value of Al, Ni and O elements of the EDS analysis (Table 7). Region 3 consists of a combination of Ni and Al and it is NiAl coating layer, where the oxide layer was detached from the surface, without any repair.

Fig. 7 illustrates the SEM micrograph of the surface of the AHHZ30 sample after 120 h cyclic oxidation at 1000 °C. As shown, a perfect and continuous oxide layer is available on the surface of the sample, without any spallation or detachment. X-ray map was obtained from the oxide scale surface after 120 h cyclic oxidation of the sample in order to evaluate the distribution of the elements (Fig. 8). The presence of oxygen, aluminum, and zirconium is related to the formation of Al_2O_3 and ZrO_2.

During the oxidation cycle, Zr may migrate toward the surface via NiAl grain boundaries where it is known to segregate. According to Fig. 7 Zr is present in the whole oxide scale and also enriched at the surface. This redistribution of Zr is consistent with the dynamic segregation of reactive elements explained by Hamadi [21] and Pint [22]. In addition, the segregation of this reactive element in the interface of the oxide and coating, as well as in the grain boundary of the oxide layer reduces the outward diffusion rate of the aluminum, leading to the growth of the oxide layer due to the inward diffusion of oxygen. Thus, the oxide scale growth mechanism is controlled by oxygen inward diffusion rather than outward diffusion of metal oxide former. In fact, Zr within the composition of coating reduces the diffusion rate of Al towards the surface of the coating as well as the consumption of Al in the coating. Therefore, the coating remains relatively stable for extended periods of time at high temperatures [5, 21-24].

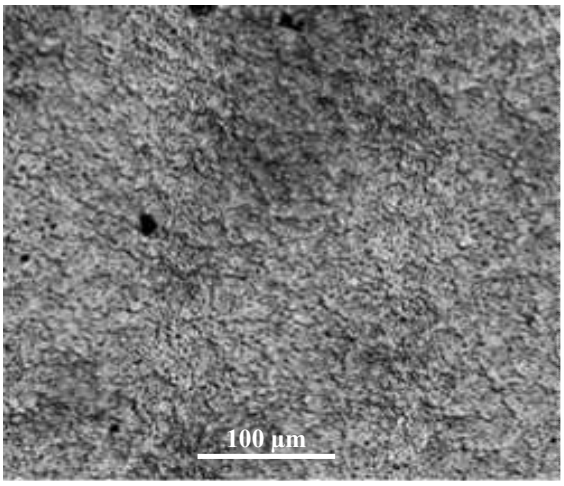

Fig. 7. SEM micrograph (Backscattered Electron) of the surface of AHHZ30 sample after 120 h cyclic oxidation at 1000°C.

[DOI: 10.22068/ijmse.16.4.63]

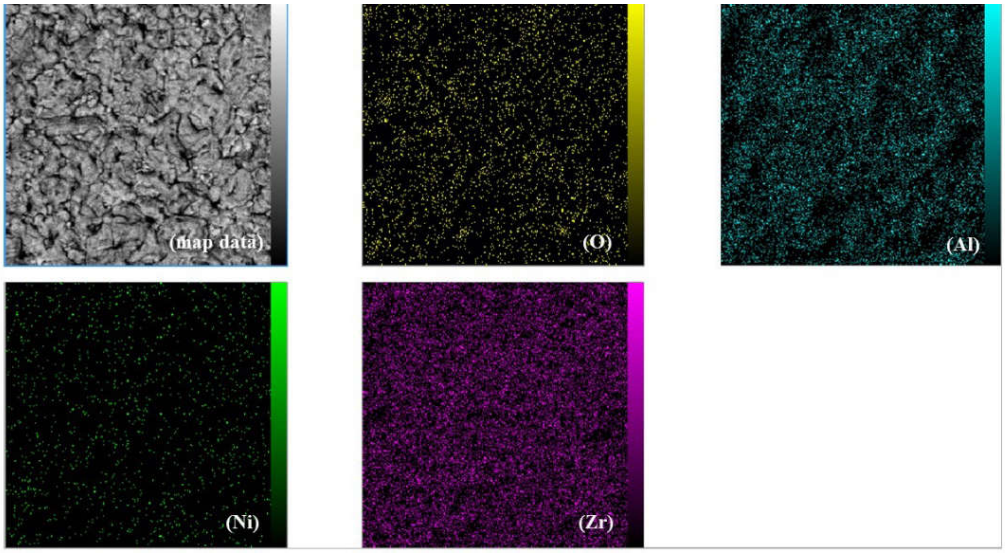

Fig. 8. X-ray map of the elements of the surface of AHHZ30 sample after 120 h cyclic oxidation at 1000°C.

Fig. 9 displays the variation of oxide layer thickness, which is measured by the cross-section of the oxide layer. As shown, an increase in the zirconium content in the coating leads to a decrease in the thickness of the oxide layer. Regarding the results of some previous studies [21, 23, 25], the reduction of the oxide layer growth rate is due to the change in the diffusion mechanism of aluminum and oxygen into the oxide scale. Further, the coating interface is considered as one of the positive effects of zirconium. In fact, the addition of zirconium leads to the selective oxidation of zirconium and aluminum since the existence of ZrO_2 at the alumina grain boundaries can act as a barrier for inward oxygen diffusion. Then, Zr in NiAl reduces the growth of oxide scale and decreases the void formation linked to cationic oxidation. Zhou [26] and Saldaña et al. [27] found that Zr containing oxides are a nucleus for α-Al_2O_3, which is beneficial for the θ to α-Al_2O_3 transformation. Since α-alumina has a slower growth rate than θ-alumina, oxide scale thickness is significantly less on NiAl coating with Zr than on simple NiAl, preventing the outward diffusion of Al in Al_2O_3 layer and the inward diffusion of oxygen leads to the growth of the oxide layer during the oxidation. Zhao et al. [28] reported that at the early stage of high-temperature oxidation, the Dy (RE) in the coating was preferentially oxidized to form Dy oxides because of its higher oxygen affinity than that of Al. According to Hwang et al. [23], the adhesion of the oxide-coat interface is improved in the presence of zirconium in the chemical composition of the coating. Based on Ellingham diagram, during the cyclic oxidation, the ZrO_2 phase is first formed because of the stronger bond between oxygen and zirconium at above 1000 °C and then it is followed by the formation of Al_2O_3 phase [29]. On the other hand, compared to the grain boundaries, aluminum and zirconium oxides, which are formed on the surface having lower diffusivity, result in reducing the oxide layer thickness. It is assumed that the addition of zirconium suppresses the transferring of aluminum cations and prevents the formation of new oxide.

Further, one of the parameters increasing the residual stresses in the oxide layer is related to its extreme growth. The stress-induced by the growing oxide layer in the zirconium modified alumina is lower than that of the unmodified alumina, due to the thinner oxide layer in the zirconium modified aluminide. As shown in Fig. 9 the thickness of 100 and 300 nm Zr modified aluminide coatings is 6 and 5 μm, respectively, while the thickness of the unmodified aluminide coating is 9 μm indicating more probability of scaling.

[DOI: 10.22068/ijmse.16.4.63]

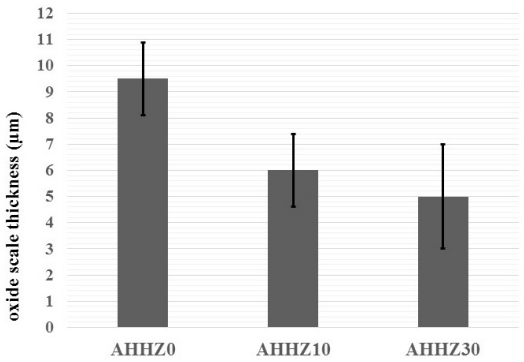

Fig. 9. The variation of oxide layer thickness for the AHHZ0, AHHZ10 and AHHZ30 samples after 120 h cyclic oxidation at 1000 °C.

By comparing the microstructures of the surface coating of the samples AHHZ0, AHHZ10 and AHHZ30 after and before oxidation, it is concluded that more spallation in the oxide layer is expected in the absence of zirconium in the coating. Therefore, the surface of the AHHZ0 sample has more scaling and spallation. Based on white regions, caused by scaling the oxide layer, the coating consists of Ni_3Al. Due to the difference between the thermal expansion coefficient of Al_2O_3 and the coating, the oxide can fail to protect the coating during thermal cycles [21]. Consequently, aluminum is diffused from the coating into the oxide layer for repair, which results in reducing aluminum content in the coating. Then NiAl coating is transformed into Ni_3Al. Thus, it is justified that spallation may be related to a mismatch between the thermal expansion coefficient of the oxide and the alloy. Generally, it is assumed that thicker oxide layers lead to a reduction in the critical stress required for the fracture. In addition, the presence of zirconium decreases the mechanical stresses, leading to a reduction in the scaling of the oxide layer during the cooling [5].

Furthermore, as shown in Table 3, based on the chemical analysis of the coating prior to the oxidation, the presence of zirconium leads to a decrease in titanium, chromium and cobalt in the coating, which may be regarded as the reason behind reducing these elements after the oxidation test in the oxide layer rather than the sample without zirconium (AHHZ0). Finally, the oxide layer is purified, leading to an increase in the adhesion to the substrate.

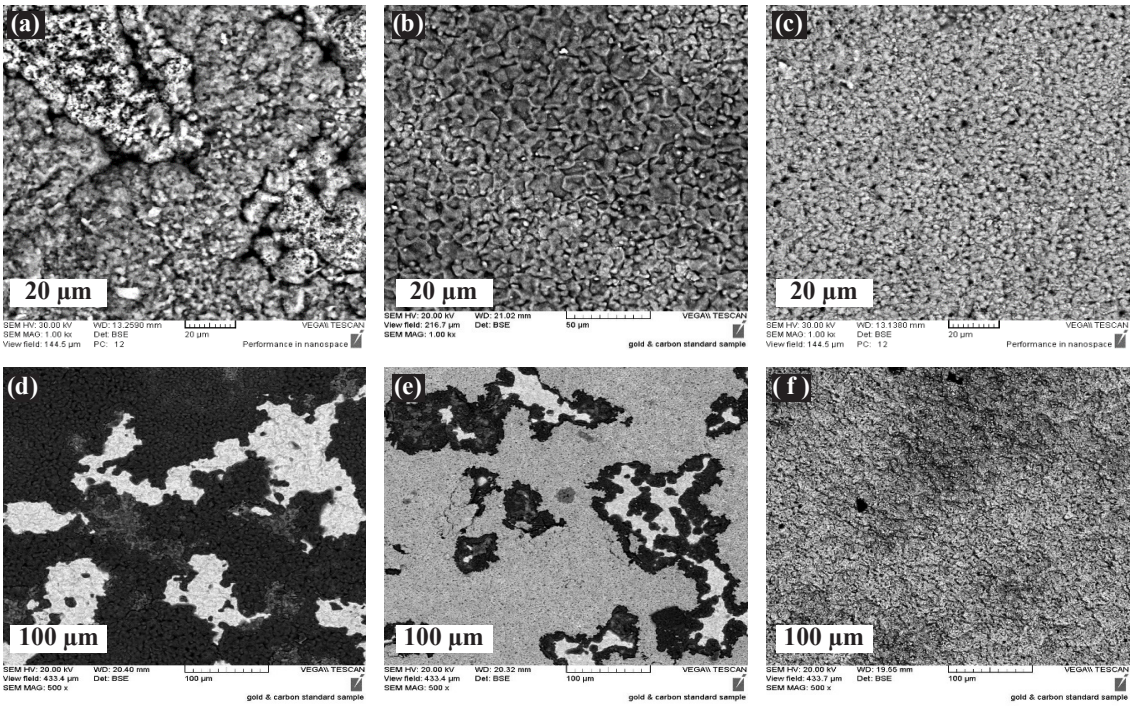

Fig. 10. SEM surface observations of the coating prior to the oxidation tests (a) AHHZ0 (b) AHHZ10 (c) AHHZ30 and the microstructure after the oxidation tests at 1000 °C for 120 hours (d) AHHZ0 (e) AHHZ10 and (f) AHHZ30.

[DOI: 10.22068/ijmse.16.4.63]

Fig. 11 illustrates the cyclic oxidation mass change data. As depicted, all the samples have a mass gain at the initial oxidation stages. However, the AHHZ0 sample including the maximum thickness of oxide layer (Fig. 9) reveals an excessive mass loss in the next steps of the oxidation process. In other words, some parts of the mentioned sample suffer from severe spallation and scaling, which is consistent with the present SEM results (Fig. 10d). Regarding AHHZ10 sample, the weight decreased after 72 h oxidation while it increased due to scale re-oxidation. As depicted in Fig. 10 (d-e), having smaller spalled areas is considered as the evidence of this mass change data, compared to AHHZ0 sample. Finally, fewer mass changes (0.2 mg/cm^2) were significantly observed in the AHHZ30 sample, indicating the slow formation rate of the adhesive and the protective oxide layer in this sample. The cyclic oxidation test confirms the results obtained from SEM surface observations of the coating in Fig. 10 (d-e).

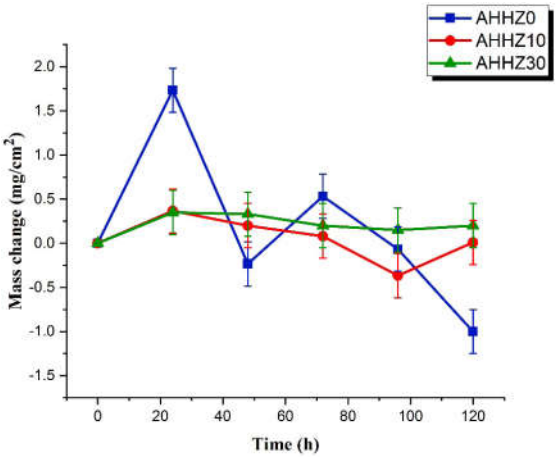

Fig. 11. Specimen mass changes curves for NiAl coating without and with zirconium modification during 120 h cyclic oxidation at 1000°C.

4. CONCLUSIONS

In the present study, like unmodified aluminide coating, Zr-modified aluminide coatings had a two-layer structure. The outer layer is composed of a uniform nickel aluminide phase and the interdiffusion layer includes a distribution of Zr in the coating layer as a solid solution. The presence of zirconium in the chemical composition of the coating caused a reduction in the content of other elements such as Ti, Co, and Cr in the oxide scale, leading to homogeneous oxide formation and better scale adhesion. The addition of Zr into the NiAl coating reduced the oxidation rate and improved the spallation resistance of the oxide scale. In addition, it could slow down the outward Al diffusion during oxidation and accordingly the growth of the aluminum oxide was restricted and caused less oxide layer thickness. The results of this study indicated that greater oxidation resistance is achieved in the case of coatings with 300 nm of zirconium, compared to the samples with 100 nm of zirconium.

REFERENCES

1. Nath, S., Manna, I., Jha, A. K., Sharma, S. C., Pratihar, S. K., Majumdar, J. D., "Thermophysical behavior of thermal sprayed yttria stabilized zirconia based composite coatings". Ceram. Int., 2017, 43, 11204–11217.
2. Du, G., Li, Z., Tan, Z., Li, G., Lin, Z., Ba, D. D., "Amping performance of YSZ coating prepared by different EB-PVD parameters". Surf. Eng., 2018, 34, 1–7.
3. Bacos, M. P., Dorvaux, J. M., Landais, S., Lavigne, O., Mévrel, R., Poulain, M., Rio, C., Vidal-Sétif, M. H., "10 years-activities at Onera". Aeorosp Lab., 2011, 3, 1–14.
4. Filip, R., Góral, M., Zawadzki, M., Nowotnik, A., Pytel, M., "The influence of long-term heat treatment on microstructure of zr-modified aluminide coating deposited by CVD method on MAR M200+Hf nickel superalloy". Key Eng. Mater., 2013, 592, 469–472.
5. Naveos, S., Oberlaender, G., Cadoret, Y., Josso, P., Bacos, M. P., "Zirconium modified aluminide by a vapour pack cementation process for thermal barrier applications: formation mechanisms and properties". Mater Sci Forum., 2004, 461, 375–382.
6. Pint, B. A., Haynes, J. A., Besmann, T. M., "Effect of Hf and Y alloy additions on aluminide coating performance". Surf. Coat. Tech., 2010, 204, 3287–3293.
7. Guo, H. B., Wang, X. Y., Ji, L. I., Wang, S. X., Gong, S. K., "Effects of Dy on cyclic oxidation resistance of NiAl alloy". T Nonferr. Metal. Soc., 2009, 19, 1185–1189.

[DOI: 10.22068/ijmse.16.4.63]

8. Shaviv, R., Roham, S. and Woytowitz, P., "Optimizing the precision of the four-point bend test for the measurement of thin film adhesion". Microelectron Eng., 2005, 82, 99–112.
9. Berndt, C. C., "Instrumented tensile adhesion tests on plasma sprayed thermal barrier coatings". J. Mater. Eng., 1989, 11, 275–282.
10. Bennett, I. J. and Sloof, W. G., "Modelling the influence of reactive elements on the work of adhesion between a thermally grown oxide and a bond coat alloy". Mat. Corr., 2006, 57, 223-229.
11. Romanowska, J, Zagula-yavorska, M, Sieniawski, J. and Markowski, J., "Zirconium modified aluminide coatings obtained by the CVD and PVD methods". O J Metal. 2013; 3: 92–99.
12. Yang, S., Wang, F. and Wu, W., "Effect of microcrystallization on the cyclic oxidation behavior of β-NiAl intermetallics at 1000 °C in air". Intermetallics., 2001, 9, 741–744.
13. Montero, X., Galetz, M. C. and Schütze, M. "Low-activity aluminide coatings for superalloys using a slurry process free of halide activators and chromates". Surf. Coat. Technol., 2013, 222, 9–14.
14. Squillace, A., Bonetti, R., Archer, N. J. and Yeatman, J. A., "The control of the composition and structure of aluminide layers formed by vapour aluminizing". Surf. Coat. Technol., 1999, 120, 118–123.
15. Benoist, J., Badawi, K. F., Malié, A. and Ramade, C., "Microstructure of Pt-modified aluminide coatings on Ni-based superalloys". Surf. Coat. Technol., 2004, 182, 14–23.
16. Qian, L., Xu, F., Voisey, K. T., Nekouie, V., Zhou, Z., Silberschmidt, V. V. and Hou, X., "Incorporation and evolution of ZrO_2 nano-particles in Pt-modified aluminide coating for high temperature applications". Surf. Coat. Technol., 2017, 311, 238–247.
17. Hwang, G. H., Choi, J. W. and Kang, S. G., "The effect of zirconium on corrosion behavior of NiAl intermetallic compound in molten carbonate salt". Z. Metal. kd., 2005, 96, 269–275.
18. Huczkowski, P., Gopalakrishnan, S. G., Nowak, W., Hattendorf, H., Iskandar, R., Mayer, J. and Quadakkers, W. J., "Effect of Zr content on the morphology and emissivity of surface oxide scales on FeCrAlY alloys". Adv. Eng. Mater., 2016, 18, 711–720.
19. Khakpour, I., Soltani, R. and Sohi, M. H., "Microstructure and High Temperature Oxidation Behaviour of Zr-Doped Aluminide Coatings Fabricated on Nickel-based Super Alloy". Proc. Mat. Sci., 2015, 11, 515–521.
20. Evans, H. E., "High Temperature Coatings: Protection and Breakdown in Shreir's Corrosion", 4th ed. Amsterdam (Netherlands): Elsevier Ltd; 2010.
21. Hamadi, S., Bacos, M. P., Poulain, M., Seyeux, A., Maurice, V. and Marcus, P., "Oxidation resistance of a Zr-doped NiAl coating thermochemically deposited on a nickel-based superalloy". Surf. Coat. Technol., 2009, 204, 756–760.
22. Pint, B. A., "Experimental observations in support of the dynamic-segregation theory to explain the reactive-element effect". Oxid. Met., 1996, 45, 1-37.
23. Hong, S., Hwang, G., Han, W., Lee, K. and Kang, S., "Effect of zirconium addition on cyclic oxidation behavior of platinum-modified aluminide coating on nickel-based superalloy". Intermetallics., 2010, 18, 864–870.
24. Zagula-Yavorska, M., Sieniawski, J. and Romanowska, J., "Oxidation behavior of zirconium-doped NiAl coatings deposited on pure nickel. Arch Mater. Sci. Eng., 2012, 58, 250–254.
25. Li, D., Guo, H., Wang, D., Zhang, T., Gong, S. and Xu, H. "Cyclic oxidation of β-NiAl with various reactive element dopants at 1200° C". Corros. Sci., 2013, 66, 125–135.
26. Zhou, Y., Zhao, X., Zhao, C., Hao, W., Wang, X. and Xiao, P., "The oxidation performance for Zr-doped nickel aluminide coating by composite electrodepositing and pack cementation". Corros. Sci., 2017, 123, 103–115.
27. Saldaña, J. M, Schulz, U., Rodríguez, G. M., Caceres-Diaz, L. A. and Lau, H., "Microstructure and lifetime of Hf or Zr doped sputtered NiAlCr bond coat/7YSZ EB-PVD TBC systems". Surf. Coat. Tech., 2018, 335, 41–51.
28. Zhao, X., Guo, H., Gao, Y., Wang, S., Gong, S., "Effects of Dy on transient oxidation behavior of EB-PVD beta-NiAl coatings at elevated temperatures". Chinese Journal of Aeronautics., 2011, 24, 363-368.
29. Balart, M. J., Patel, J. B., Gao, F. and Fan, Z., "Grain refinement of deoxidized copper". Metall. Mater. Trans. A., 2016, 47, 4988–5011.

[DOI: 10.22068/ijmse.16.4.63]